High temperature oxidation resistance of (Ti,Ta)(C,N)-based cermets

E. Chicardi*[1,2], J.M. Córdoba[1,3] and F. J. Gotor[1]

[1]Instituto de Ciencia de Materiales de Sevilla (CSIC-US), Américo Vespucio 49, 41092 Sevilla, Spain.

[2]Departamento de Ingeniería Metalúrgica y de Materiales, Universidad Técnica Federico Santa María, Valparaíso 1680, Chile.

[3]Departamento de Química Inorgánica, Universidad de Sevilla (US), Calle Prof. García González 1, 41012, Sevilla, Spain

Abstract

Cermets based on titanium-tantalum carbonitride were oxidized in static air between 800 ºC and 1100 ºC for 48 h. The thermogravimetric and microstructural study showed an outstanding reduction in the oxidation of more than 90% when the Ta content was increased. In cermets with low Ta content, the formation of a thin CoO/Co_3O_4 outer layer tends to disappear by reacting with the underlying rutile phase, which emerges at the surface. However, in cermets with higher Ta content, the formation of an external titanate layer, observed even at a low temperature, appears to prevent the oxygen diffusion and the oxidation progression.

Keywords: A. Ceramic matrix composites; A. Cobalt; A. Titanium; B. SEM; B. X-ray diffraction; C. Oxidation.

* Corresponding Author. Tel: +34 954489217. Fax: +34 954460165. E-mail: echicardi82@gmail.com / ernesto.chicardi@icmse.csic.es

1. Introduction.

The materials used in various applications, such as cutting tools (rock and earth drilling tools), drawing and sheet metal-forming tools and dies, wear parts (nozzles, plunges, paper cutters, etc.) and other structural components (mechanical seals, boring

bars, etc.), can encounter extreme conditions (high temperature, pressure, and an oxidizing atmosphere, among others) during use. For this reason and because of constantly increasing industrial demands, the search for novel materials and designs with improved performance remains a challenge. Materials for these applications are expected to possess not only high abrasive and impact wear resistance but also excellent high temperature corrosion or/and oxidation resistance. Oxidation in non-oxidic structural materials is a major disadvantage because it typically controls the operational properties. Oxidation can reduce ductility, tensile strength and erosion and corrosion resistance, among other properties [1-3]. Oxidation is not always a slow process and can progress significantly over a short service time in certain practical applications [4].

Hard materials used in the metal working industry for high-speed machining must withstand a broad range of thermal, mechanical and chemical stresses. These materials are primarily based on tungsten carbide (cemented carbides) or titanium carbonitride (cermets). The desired properties can be achieved through complex alloying with other transition metals, such as Ta and Nb [5-7]. In this context, (Ti,Ta)(C,N)-based cermets have been successfully utilized as heat-resistant structural materials, including wear parts and, especially, cutting tools in high-speed finishing and semi-finishing applications due to their excellent physical and chemical properties, such as a favorable hot hardness, excellent wear resistance, perfect chemical stability, low friction coefficient to metals and great thermal deformation resistance [8-15]. However, while in service, (Ti,Ta)(C,N)-based cermets are often exposed to elevated temperatures in oxidizing environments [16]; therefore, their oxidation behavior plays a key role in cutting performance and tool life.

In a previous study [17], it was determined at a fixed temperature of 900 ºC that the oxidation resistance of the (Ti,Ta)(C,N)-based cermets was significantly dependent on the Ta content. The goal of the present work is to report a systematic study of the outstanding oxidation improvement of $Ti_xTa_{1-x}C_{0.5}N_{0.5}$-Co cermets over a wide temperature range (800 ºC-1100 ºC) to address the lack of available experimental data in the literature on this topic. This study also attempts to provide new insights into the key role played by Ta in the excellent oxidation resistance of cermets. Note that the temperatures studied cover the maximum cutting tool work temperatures for the most demanding processes [18]. It must be considered that cutting tool oxidation at these

temperatures is more important than the mechanical abrasion in determining the tool life in many cases.

2. Experimental.

Five cermets with nominal compositions of 80 wt% $Ti_xTa_{1-x}C_{0.5}N_{0.5}$ – 20 wt% Co and variable Ta atomic content, x = 1, 0.99, 0.95, 0.90 and 0.80 (labeled as **Ti100**, **Ti99Ta1**, **Ti95Ta5**, **Ti90Ta10** and **Ti80Ta20**, respectively), were synthesized by the mechanochemical process called the Mechanically Induced Self-Sustaining Reaction (MSR) from Ti, Ta and C powder mixtures and N_2 gas. A powder mixture containing 46.5 g elemental Ti (99% purity, <325 mesh, Strem Chemicals), Ta (99.6% purity, <325 mesh, Alfa-Aesar), C (as graphite, <270 mesh, Fe < 0.4%, Merck) and Co (99.8% purity, <100 mesh, Strem Chemicals), together with 13 tempered steel balls (d = 20 mm, m = 32.6 g), were put into a tempered steel vial (300 ml in volume) and milled using a modified planetary ball mill (P4, Fritsch) at a spinning rate of 400 rpm under 6 atm N_2 gas (H_2O and O_2 < 3 ppm, Air Liquide). The planetary ball mill enabled the MSR reactions to be monitored by continuously measuring the pressure inside the vial. When the MSR reaction associated with the synthesis of the $Ti_xTa_{1-x}C_{0.5}N_{0.5}$ carbonitride solid solution phase occurs, the temperature increases due to the release of heat from the exothermic formation reaction, which consequently increases the total pressure. The ignition time, i.e, critical milling time required to induce the MSR process, can then be determined from the spike in the recorded time-pressure data. After ignition, the milling is continued to ensure full conversion and homogenization. The ignition time was about 45 min for all cermets and the total milling time was 75 min.

Subsequently, the powdered cermets were shaped using a uniaxial press (2 tons, 5 min) and compacted by cold isostatic pressing (200 MPa, 10 min). The green bodies were then sintered at temperatures between 1450 ºC and 1550 ºC, optimized for each Ta/Ti ratio [19], for 60 min under a flowing Ar (H_2O < 3 and O_2 < 2 ppm, Linde) atmosphere in a horizontal tubular furnace (IGM1360 model No. RTH-180-50-1H, AGNI) to obtain cylindrical cermets 13 mm in diameter and 9 mm in height. After sintering, the cermets consisted of the mentioned carbonitride phase ($Ti_xTa_{1-x}C_{0.5}N_{0.5}$) and two Ti-Ta-Co intermetallic compounds, namely, $Ti_xTa_{1-x}Co_2$ and $Ti_xTa_{1-x}Co$, acting

as binder instead of the initial Co. A detailed description of the microstructure and properties of cermets can be found in a previously published study [19].

To perform the oxidation experiments, parallelepiped specimens of these five sintered cylinder cermets with similar dimensions (3±0.1 mm x 4±0.1 mm x 5±0.1 mm) and surface area (94±0.5 mm^2) were obtained by cutting from the center part of the sintered body. The surfaces of cermets were subjected to successive grinding and polishing steps (final step with 3 μm diamond powder suspension). Finally, the specimens were ultrasonically cleaned with ethanol. The oxidation tests were performed in static air under isothermal conditions from 800 ºC to 1100 ºC (heating rate of 20 ºC/min and free cooling) for 48 h. The weight gain due to oxidation was continually monitored using a CI Robal electrobalance (C.I. Electronics Ltd.) with a maximum weight allowed of 5 g and a sensitivity of 1 μg; the balance was attached to the support frame of a high-temperature vertical furnace (Severn Thermal Solutions Ltd.) designed for use up to 1500 ºC. The specimens were placed on a platinum wire coil to maximize the contact of the surfaces with the surrounding atmosphere.

X-ray diffraction (XRD) diagrams were collected on the surfaces exposed to oxidation to get information about the phases present in the oxide scale of the oxidized cermets. XRD patterns were also obtained once the oxidized specimens (bulk + oxide scale) were crushed and reduced to powder by hand-grinding to obtain information on the extent of oxidation. A PANalytical X'Pert Pro instrument equipped with a θ/θ goniometer, a Cu K_α radiation source (40 kV, 40 mA), a secondary K_β filter and an X'Celerator detector was used. The diffraction patterns were collected from 20º to 80º (2θ) in a step-scan mode at a step of 0.02º and a counting time of 275 s/step and were compared with those in the PDF-4+ database from the International Centre for Diffraction Data (ICDD). Lanthanum hexaboride powder (Standard Reference Material for powder diffraction 660b, NIST) was used to calibrate the positions of the diffraction lines. Lattice parameters were calculated from the complete set of peaks in the XRD pattern using the DICVOL04 software.

The polished cross sections of the oxidized specimens were examined via scanning electron microscopy (SEM) performed on a Hitachi S-4800 SEM-FEG microscope coupled with an X-ray energy dispersive spectrometry (XEDS) detector

(Quantax-EDS, Bruker Corporation), which was used for the chemical semiquantification of the ceramic, binder and oxidized phases.

3. Results and Discussion.

3.1. Dependence of oxidation on temperature and tantalum content.

The weight gain normalized to the surface area of the material (per unit area) after 48 h of oxidation for all of the temperatures and cermets is shown in figure 1. A significant decrease in the extent of oxidation is clearly observed for all of the temperatures when the Ta content is increased. Cermet without Ta (**Ti100**) exhibited a non-negligible oxidation (18.6 mg/cm^2), even at the lowest oxidation temperature tested (800 ºC). However, cermet **Ti90Ta10** with a higher Ta content required a substantially higher temperature (1100 ºC) to produce a similar oxidation level (19.5 mg/cm^2). At 1100 ºC, cermet **Ti80Ta20** showed a low oxidation of 9.5 mg/cm^2, which was lower than that of cermet **Ti100** at 800ºC. At 800 ºC, the oxidation of cermets **Ti95Ta5**, **Ti90Ta10** and **Ti80Ta20** was practically imperceptible. In contrast, cermets **Ti100** and **Ti99Ta1** were extensively oxidized at 1100 ºC.

To quantify the improvement in the oxidation resistance of cermets when Ti is partially substituted by Ta, the percentage reduction of the weight gain per unit area for each cermet at each temperature using the **Ti100** cermet as reference is presented in table 1. By replacing only 1 at% of Ti with Ta (**Ti99Ta1**), oxidation was reduced by 67.2% at 800ºC. This improvement remained high for **Ti99Ta1** until 1100 ºC (46.3%). At this high temperature, the enhancement of oxidation resistance increases with increasing Ta content, reaching a remarkable 92.8% for **Ti80Ta20**. An improvement of at least 90% is also achieved in cermets **Ti95Ta5** and **Ti90Ta10** but at lower temperatures of 900 ºC and 1000 ºC, respectively.

To corroborate the thermogravimetric results and to analyze the phases formed during the oxidation tests, XRD patterns of oxidized cermets reduced to powder are compared in figure 2. The XRD pattern corresponding to oxidized **Ti100** cermet at a low temperature (800 ºC) clearly shows the presence of rutile TiO_2 (tetragonal structure, P42/mnm, 136) due to the cermet oxidation. The intensity of the TiO_2 reflections increases with the oxidation temperature as the oxidation progresses. Moreover, new

reflections that can be assigned to cobalt methatitanate ($CoTiO_3$, rhombohedral structure, R-3, 148) are detected from 900 ºC. The existence of this Co-containing phase is due to the presence of Co in the binder phase, which is also oxidized. Simultaneously, the intensity of the original ceramic and binder phases is considerably reduced. At 1000 ºC, the unoxidized phases are only slightly detected in the XRD patterns, suggesting a high degree of oxidation, in accordance with the thermogravimetric results. At 1100 ºC, the XRD pattern is practically dominated by the TiO_2 rutile reflections. Note that as described in the literature [19], the binder phase in cermets developed by MSR was composed of a mixture of TiCo (cubic structure, Pm-3m, 221) and $TiCo_2$ (cubic structure, Fd-3m, 227) intermetallic phases. Therefore, the presence in the oxidized specimen XRD patterns of reflections corresponding to a α-Co alloy (cubic structure, Fm-3m, 225) implies the preferential oxidation of Ti vs Co in the binder phase.

The XRD patterns of oxidized **Ti99Ta1** cermet (figure 2) show a similar trend to that of **Ti100** cermet as the oxidation progresses with temperature. However, the improvement in the oxidation resistance by substituting only 1 at% of Ti with Ta is evidenced by the delay in the evolution of oxidized phases, corroborating the thermogravimetric results in figure 1. A comparison of the XRD patterns of the oxidized cermets reveals that the patterns are similar but shifted by 100 ºC, e.g., XRD patterns at 900 ºC, 1000 ºC and 1100 ºC for **Ti99Ta1** cermet are equivalent to those at 800 ºC, 900 ºC and 1000 ºC for **Ti100** cermet, respectively. This result indicates that oxidation was deferred by approximately 100 ºC.

For **Ti95Ta5** cermet, the XRD patterns in figure 2 indicate that the oxidation remained at a low level until 1100 ºC in which the reflections of the original unoxidized phases were still clearly visible. The XRD pattern of **Ti95Ta5** cermet at 1100 ºC was similar to that of **Ti99Ta1** and **Ti100** cermets at 900 ºC and 800 ºC, respectively, showing again the positive effect of Ta substitution on oxidation resistance. In this case, when Ti was replaced with 5 at% of Ta, the oxidation was delayed by approximately 300 ºC compared with cermets without Ta.

For **Ti90Ta10** and **Ti80Ta20** cermets, with the highest Ta contents of 10 and 20 at%, respectively, the XRD patterns in figure 2 show an even greater oxidation resistance. The XRD patterns of **Ti80Ta20** cermet are dominated by the unoxidized

phases over the entire temperature range studied. Only at 1000 ºC, the most intense reflections of the rutile structure begin to emerge from the background signal.

Note that single tantalum oxides, such as Ta_2O_5 or TaO_2, were not detected in the XRD patterns of oxidized cermets (figure 2). However, displacements toward the lower 2θ angles were observed in the reflections corresponding to the rutile structure when the Ta amount was increased. This effect is illustrated in figure 3 in which the XRD patterns over the range of the (110) and (211) reflections for TiO_2 and TaO_2 are shown for the five different cermets oxidized at 1100 ºC. The observed shift is equivalent to an increase in the unit cell parameters as shown in table 2 and suggests that Ta is introduced into the TiO_2 lattice, resulting in the formation of a $Ti_xTa_{1-x}O_2$ solid solution with rutile-type structure (tetragonal structure, P42/mnm, 136).

3.2. Surface characterization of the oxidized cermets.

To obtain precise information on the nature of the oxide scale formed in oxidized cermets, XRD patterns of the surfaces exposed to oxidation were recorded and are shown in figure 4. In the XRD pattern of **Ti100** cermet oxidized at 800 ºC, CoO (cubic structure, Fm-3m, 225) and Co_3O_4 (cubic structure, Fd-3m, 227) are the only phases observed. However, these oxides were not detected at this temperature in the XRD pattern of figure 2 in which only unoxidized phases and low intensity peaks corresponding to TiO_2 were identified. These differences are due to the penetration depth of the X-ray and the fact that both of the cobalt oxides must be located precisely at the outermost layer of the oxide scale, preventing the detection of other inwardly located phases. At 900 ºC, CoO appears as the major phase because of the instability of Co_3O_4, according to reaction (1), although the marked (200) preferred orientation observed (2θ ≈ 42.4º) could also be at the origin of this predominance in the XRD pattern.

$$2\,Co_3O_4 \quad \Leftrightarrow \quad 6\,CoO + O_2 \qquad (1)$$

Note that the presence of external CoO and Co_3O_4 implies the migration of cobalt through the TiO_2 oxide layer, which is supposed to be the main product of oxidation, towards the surface of cermets and its subsequent oxidation. The formation of an outermost region of nearly pure cobalt oxide has been frequently observed during the oxidation of Co-base alloys [20, 21].

At higher temperatures (1000 ºC and 1100 ºC) (figure 4), when the oxidation has significantly progressed, TiO_2 emerges at the surface of the cermet, while cobalt oxides disappear by reacting with TiO_2 rutile to form cobalt methatitanate ($CoTiO_3$) or cobalt orthotitanate (Co_2TiO_4, cubic structure, Fd-3m, 227), according to reactions (2-5), as follows [22, 23]:

$$CoO + TiO_2 \Leftrightarrow CoTiO_3 \quad (2)$$

$$2\,Co_3O_4 + 6\,TiO_2 \Leftrightarrow 6\,CoTiO_3 + O_2 \quad (3)$$

$$2\,CoO + TiO_2 \Leftrightarrow Co_2TiO_4 \quad (4)$$

$$2\,Co_3O_4 + 3\,TiO_2 \Leftrightarrow 3\,Co_2TiO_4 + O_2 \quad (5)$$

It is possible to consider the formation of Co_2TiO_4 from $CoTiO_3$, according to the following reaction (6):

$$CoO + CoTiO_3 \Leftrightarrow Co_2TiO_4 \quad (6)$$

The XRD patterns of oxidized surfaces of **Ti99Ta1** cermet (figure 4) are generally similar to those corresponding to **Ti100** cermet (with the same shift in temperature as previously observed in figure 2), although certain differences are also noticed. The first difference is the presence of rutile and small reflections of cobalt titanates ($CoTiO_3$ and Co_2TiO_4) at 800 ºC. For **Ti99Ta1** cermet, cobalt oxides dominate the XRD pattern of the surface at higher temperatures, over the 900-1000 ºC temperature range. Second, the XRD pattern of the oxidized surface at 1100 ºC shows the presence of intense reflections of Co_2TiO_4 and $CoTi_2O_5$ (orthorhombic structure, Cmcm, 63). This result is in contrast to the pattern for **Ti100** cermet at this temperature in which only TiO_2 was detected. According to the binary CoO/Co_3O_4-TiO_2 phase diagram [22], cobalt dititanate ($CoTi_2O_5$) is stable at temperatures above ~1140 ºC, and its formation at these temperatures can occur by reactions (7-10), as follows:

$$CoTiO_3 + TiO_2 \Leftrightarrow CoTi_2O_5 \quad (7)$$

$$CoO + 2\,TiO_2 \Leftrightarrow CoTi_2O_5 + O_2 \quad (8)$$

$$2\,CoTiO_3 \Leftrightarrow CoTi_2O_5 + CoO \quad (9)$$

$$3\,TiO_2 + Co_2TiO_4 \;\Leftrightarrow\; 2\,CoTi_2O_5 \qquad (10)$$

The existence of a higher proportion of cobalt titanates, especially Co_2TiO_4, at lower temperatures becomes more apparent with increasing Ta content (**Ti95Ta5**, **Ti90Ta10** and **Ti80Ta20** in figure 4). These observations suggest that the substitution of Ti^{4+} by Ta^{5+} in the rutile phase and the formation of Ti^{3+} in the structure for charge compensation [24] must increase the reactivity of this phase and promote the formation of cobalt titanates at lower temperatures through reactions (2-5). Moreover, note that cobalt oxides (CoO and Co_3O_4) were not observed in the oxidized surfaces of **Ti90Ta10** and **Ti80Ta20** cermets over the entire temperature range studied. For both of the cermets, only the rutile, Co_2TiO_4 and $CoTiO_3$ phases are observed. It is then possible to propose for these cermets the direct reaction between cobalt and rutile to produce cobalt titanates at the surface through reactions (11 and 12) instead of reactions (2-5). The stoichiometries proposed in reactions (11 and 12) are based on the XEDS results by SEM (shown later), showing that cobalt titanates do not contain Ta and revealing the existence in the same specimen of a $Ti_xTa_{1-x}O_2$ solid solution with different Ti/Ta ratios.

$$Co + Ti_xTa_{1-x}O_2 + 1/2\ O_2 \;\Leftrightarrow\; CoTiO_3 + Ti_yTa_{1-y}O_2 \qquad (11)$$

$$2Co + Ti_xTa_{1-x}O_2 + O_2 \;\Leftrightarrow\; Co_2TiO_4 + Ti_yTa_{1-y}O_2 \qquad (12)$$

The XRD pattern in figure 4 for the **Ti80Ta20** cermet at 1100 ºC only shows the presence of Co_2TiO_4 and $CoTiO_3$. Maintaining these cobalt titanates as an outermost layer in the oxide scale at higher temperatures should be related to the improvement in oxidation resistance of cermets and would indicate a more protective effect than that provided by the rutile layer only. Furthermore, it has been shown that Ta^{5+} doping in the rutile phase decreases the oxygen vacancy concentration, hindering the oxygen mass transport [25] through the oxide scale, which should also decelerate the oxidation of cermets [26].

Finally, note that except for **Ti80Ta20** oxidized at 800 ºC, the XRD patterns of oxidized surfaces for **Ti90Ta10** and **Ti80Ta20** cermets do not show the presence of unoxidized phases, although TG measurements evidenced a low degree of oxidation. This fact is related again to the penetration depth of the X-rays that as confirmed by

SEM observations (figure 5) was about 10 μm in the present case; thus, the phases present below this depth are unlikely to be detected.

3.3. Characterization of oxides and subsurfaces in cross-sections by SEM.

To study how oxygen penetrates cermets and to study the distribution and composition of phases from the external surface of the oxide scale to the inner part of the different specimens, polished cross-sections of oxidized cermets were analyzed by SEM. Considering the large number of samples and the wide range of oxidation temperatures studied, only the more representative results are presented in this section.

Figure 5 shows an example of the cross-sectional SEM images of the different cermets oxidized at 800 ºC, clearly showing the drastic reduction in oxidation depth as the Ta content is increased from 220 μm for **Ti100** to 6 μm for **Ti80Ta20** (note the different magnification in the SEM images). This result confirms the outstanding improvement of oxidation resistance when Ta is introduced into the structure of the carbonitride phase. The same trend was observed with increasing temperature, although for the same Ta content, the volume affected by oxidation also increases with temperature (figure 6).

The SEM images in figures 5 and 6 show that the volume affected by oxidation can be divided into two primary regions, which is more clearly visible in specimens with a higher oxidation. For example, in **Ti100** cermet oxidized at 800ºC, a large external zone, approximately 147 μm wide, only composed of oxidized phases (as confirmed by XEDS-SEM mapping) is observed (figure 7). The large pores observed in this region were presumably generated by coalescence of smaller pores formed because of the volatile species arising from the oxidation of the carbonitride phase. Immediately below this region, there is a partially oxidized internal degradation zone with lower porosity. The width of this layer (~ 73 μm) and its depth imply an important diffusion of oxygen into the cermet, which suggests a limited protection of the formed oxide scale. When Ta is introduced into cermets, both of the regions experienced a significant reduction in thickness, especially the internal degradation zone in cermets with a higher Ta content. Simultaneously, the porosity of the fully oxidized external layer was drastically reduced with the Ta content, which may contribute to increased oxidation protection.

Analytical measurements using XEDS-SEM performed at different locations (marked with numbers in figures 8-10) were obtained to gain additional information for the identification of the different phases present in the oxide scale and the internal degradation zone of oxidized specimens. Representative semi-quantitative compositions obtained from XEDS-SEM spectra (some characteristic ones are displayed in figure 11) are shown in table 3 and the calculated Ti/Ta/Co/O atomic ratios were used to assign the different phases previously detected by XRD to the different areas analyzed. So, the formation at low temperatures of a thin external layer composed of CoO and Co_3O_4 was confirmed for the **Ti100** cermet (numbers 1 and 2, respectively, in figure 8a, corresponding to the outermost zone of **Ti100** cermet oxidized at 800 ºC). Immediately below this layer, the TiO_2 phase was detected (number 3 in figure 8a), along with $CoTiO_3$ (number 4 in the same figure 8a). The irregular morphology present in this phase and the location of $CoTiO_3$ between cobalt and titanium oxides support its formation according to reactions (2) and (3). Subsequently, a Co-depleted zone was detected, and further from the surface, $CoTiO_3$ was again detected (figure 8a). In this case, this phase could have been directly formed through reaction (11).

At a higher temperature (1000 ºC), when the oxidation has significantly progressed, the SEM image of the external oxidation zone of **Ti100** cermet reveals the absence of cobalt oxides at the surface and the emergence of TiO_2 (number 3 in figure 8b). The existence of $CoTiO_3$ is also observed in figure 8b (number 4) because of reactions (2) and (3) that would have consumed cobalt oxides formed in an earlier oxidation stage. Note that although Co_2TiO_4 was assigned in the superficial XRD pattern (figure 3), it could not be detected by XEDS-SEM. The presumably low amount of this phase, the fine scale of the microstructure and the interference from neighboring phases can cause difficulty in distinguishing between the $CoTiO_3$ and Co_2TiO_4 phases.

For **Ti99Ta1** cermet, a similar phase distribution to that for **Ti100** was found in the superficial oxidation zone. The formation of the external cobalt oxide layer (numbers 1 and 2 in figure 8c) was confirmed at 800 ºC and was still observed at 1000 ºC (figure 8d); this layer only disappeared at 1100 ºC (figure 8e). At this temperature, the rutile phase (number 3) emerges at the surface of the oxidized cermet. $CoTiO_3$ was also detected near the cobalt oxide layer at the lower oxidation temperature, and Co_2TiO_4 and $CoTi_2O_5$ were evidenced at a high temperature (1100 ºC) (numbers 5 and 6, respectively, in figure 8e).

The trend to form cobalt titanates instead of cobalt oxides at low oxidation temperatures when Ti is increasingly substituted by Ta is illustrated for **Ti95Ta5** cermet in figure 9a. The chemical compositions determined by XEDS-SEM in the outermost layer of the oxide scale formed at 900 ºC (numbers 4 and 5 in figure 9a) were in agreement with the XRD results (figure 4), in which the $CoTiO_3$ and Co_2TiO_4 phases were detected in the surface of oxidized **Ti95Ta5** cermet. At the highest oxidation temperature, 1100 ºC, the cobalt titanate layer ($CoTiO_3$ and Co_2TiO_4) remained at the surface (figure 9b). At this temperature, a small external layer of CoO was observed (number 1 in figure 9b) in some specific areas. The cobalt titanate layer was only 10 microns thick, and it was continuous and dense; the emergence of the rutile phase at the external surface of the cermet was never demonstrated.

For **Ti90Ta10** and **Ti80Ta20** cermets, it was confirmed that a cobalt titanate layer was always formed and was retained at the surface over the entire oxidation temperature range studied (800-1100 ºC), as exemplified in figures 9c and 9d for **Ti90Ta10** cermet oxidized at 800 ºC and **Ti80Ta20** cermet at 1000 ºC, respectively. This cobalt titanate layer in the **Ti90Ta10** and **Ti80Ta20** cermets appears to be composed of the superposition of two continuous oxides. Co_2TiO_4 was observed in the outermost zone, and $CoTiO_3$ appeared immediately below it (numbers 5 and 4, respectively, in figure 9d). The complete absence of cobalt oxides (CoO and Co_3O_4) at each oxidation temperature confirms that titanates were formed directly between Co and $Ti_xTa_{1-x}O_2$ according to reactions (11) and (12). However, the thickness of this titanate layer increased with the oxidation temperature because of the oxidation progress but only slightly, as shown in figures 9c and 9e for **Ti90Ta10** cermet oxidized at 800 ºC and 1000 ºC, respectively. Under this titanate top layer, a $Ti_xTa_{1-x}O_2$ sublayer was observed (number 3 in figure 9). This layer was thin due to the small degree of oxidation, thus preventing the accumulation of compressive stresses and avoid the cracking of the protective titanate layer, which maintains its integrity by remaining dense and continuous.

Note that the presence of Ta in the rutile phase was ascertained by XEDS-SEM, confirming the formation of a $Ti_xTa_{1-x}O_2$ solid solution, whereas Ta was never observed in any of the titanate phases. This result appears to indicate that it is impossible to form a solid solution for these mixed oxides, probably due to the different structures and

compositions of cobalt tantalates ($CoTa_2O_6$ and $Co_4Ta_2O_9$, according to the PFD-ICDD database) compared with cobalt titanates.

Moreover, note that XEDS-SEM measurements revealed the existence of a chemical gradient in the $Ti_xTa_{1-x}O_2$ solid solution, which becomes more apparent with increasing Ta content. A composition virtually without Ta was observed near the surface, while moving inwards, the amount of Ta increased in the solid solution. As an example, in figure 9b corresponding to the **Ti80Ta20** cermet oxidized at 800 ºC, the numbers 3a, 3b and 3c represent the $Ti_xTa_{1-x}O_2$ solid solution but with three different Ti/Ta atomic ratios of ~ 16, 5.3 and 2.4, respectively, determined from the Ti and Ta atomic percentages obtained from XEDS-SEM analysis. Note that this last ratio is even lower than the starting nominal ratio of 4 in the carbonitride phase ($Ti_{0.8}Ta_{0.2}C_{0.5}N_{0.5}$). These results account for a faster diffusion of Ti toward the external surface to be oxidized compared with Ta, which could also explain the absence of Ta in cobalt titanates.

The chemical characterization of the internal degradation zone of the different oxidized cermets confirmed that it was always composed of a continuous rutile matrix in which isolated rounded packets of a Co alloy are embedded. As previously mentioned, this area was dramatically reduced as the Ta content increased and was extremely small and difficult to observe for cermets with the highest Ta content at any of the oxidation temperatures studied. Figures 10a, 10b and 10c show this zone for cermets **Ti100** oxidized at 1000 ºC, **Ti99Ta1** at 1000 ºC and **Ti95Ta5** at 1100 ºC, respectively.

Semiquantitative analysis by XEDS-SEM performed in the Co alloy pockets (number 7 in figures 10a, 10b and 10c) always revealed a Co content higher than 90 at% (Ti and Ta were the other metallic elements detected in the alloy). Because the original binder phases had a markedly higher Ti and Ta content (see ref. [19]), these XEDS-SEM analyses confirm that a preferential oxidation of Ti and Ta occurred in the binder phase.

Finally, after the internal degradation zone and immediately before reaching the unoxidized phases, a new narrow layer that corresponds to the oxidation front was observed. In this region, the incipient oxidation of the cermet occurs, and phases in the Ti-Ta-Co-O system were detected with chemical compositions close to the ceramic and

binder phases but with a non-negligible amount of oxygen. As an example, in figure 10d, the oxidation front in the **Ti100** cermet oxidized at 900 ºC is shown. In figures 5-7 the oxidation front in oxidized cermets can also be observed.

Figure 10e shows details of the oxidation front of the **Ti80Ta20** cermet oxidized at 1100 ºC. This image and XEDS-SEM analyses performed at different points of the reaction front allowed the conclusion that the onset and advancement of the oxidation reaction occurs at the level of the binder phase by the preferential oxidation of Ti and Ta. Subsequently, oxidation proceeds towards the ceramic particles, leading to the characteristic microstructure of the internal degradation zone, with Co as the last element to be oxidized in cermets.

4. Conclusions.

1. The substitution of Ti by Ta in titanium carbonitride-based cermets results in an extraordinary improvement of the oxidation resistance. This improvement was observed over the entire temperature range studied (800 ºC-1100 ºC). The improvement was especially remarkable in **Ti80Ta20** cermet, for which oxidation was reduced by more than 90%.

2. The oxidized zone can be divided in three regions, as follows: a) an external oxide scale in which fully oxidized phases coexist, such as cobalt oxides (CoO and Co_3O_4), titanium-tantalum oxide with the rutile-type structure ($Ti_xTa_{1-x}O_2$) and cobalt titanates ($CoTiO_3$, Co_2TiO_4 and $CoTi_2O_5$), depending on the temperature and Ta content; b) a partially oxidized internal degradation zone in which $Ti_xTa_{1-x}O_2$ and α-Co coexist; and c) the oxidation front in which the incipient oxidation of the ceramic and binder phases occurs. The oxide scale and the internal degradation zones are significantly reduced when the Ta content is increased in cermets.

3. For the cermets with zero or low Ta content, **Ti100** and **Ti99Ta1**, the degree of oxidation is important, even at low temperatures, and the formation in the oxide scale of a thin CoO/Co_3O_4 external layer is observed. When the oxidation temperature is increased, these cobalt oxides react with the underlying rutile phase to form cobalt titanates. The cracking of the CoO/Co_3O_4 external layer induces the emergence of the rutile phase at the surface of the oxide scale.

4. For the cermets with higher Ta content, **Ti95Ta5**, **Ti90Ta10** and **Ti80Ta20**, the formation of a cobalt titanate external layer instead of the CoO/Co_3O_4 layer is observed, even at the lowest oxidation temperature studied. This external layer remains stable at increasing oxidation temperatures.

5. The improved oxidation resistance observed with Ta substitution arises from a synergic effect that includes the lower tendency of Ta to oxidize, the formation of a continuous and compact protective layer of cobalt titanate at the surface of the oxide scale and the formation of a $Ti_xTa_{1-x}O_2$ solid solution with rutile-type structure in which some Ti^{4+} are replaced by Ta^{5+}, which reduces oxygen vacancies and then the oxygen diffusion into cermets.

Acknowledgments.

This study was supported by the Spanish Government under grant MAT2011-22981, financed in part by the European Regional Development Fund of 2007-2013. E. Chicardi and J. M. Córdoba were supported by CSIC through the JAE-Pre and JAE-Doc grants, respectively, which are financed, in part, by the European Social Fund (ESF).

References.

[1] J. Nicholls, Advances in coating design for high-performance gas turbines, Mrs Bulletin, 28 (2003) 659-670.
[2] K.J.A. Brookes, Hardmetals and Other Hard Materials, International Carbide Data, 1992.
[3] W.B. Eisen, B.L. Ferguson, R.M. German, R. Iacocca, P.W. Lee, D. Madan, K. Moyer, H. Sanderow, Y. Trudel, ASM Handbook Volume 7: Powder Metal Technologies and Applications, ASM International, 1998.
[4] J. Pujana, L. del Campo, R.B. Perez-Saez, M.J. Tello, I. Gallego, P.J. Arrazola, Radiation thermometry applied to temperature measurement in the cutting process, Measurement Science & Technology, 18 (2007) 3409-3416.
[5] M. Naidoo, O. Johnson, I. Sigalas, M. Herrmann, Influence of tantalum on the microstructure and properties of Ti(C,N)-Ni cermets, International Journal of Refractory Metals & Hard Materials, 42 (2014) 97-102.
[6] J.M. Córdoba, M.A. Avilés, M.J. Sayagués, M.D. Alcalá, F.J. Gotor, Synthesis of complex carbonitride powders TiyMT1-yCxN1-x (MT:Zr,V,Ta,Hf) via a mechanically induced self-sustaining reaction, Journal of Alloys and Compounds, 482 (2009) 349-355.
[7] U. Rolander, G. Weinl, M. Zwinkels, Effect of Ta on structure and mechanical properties of (Ti,Ta,W)(C,N)-Co cermets, Int. J. Refract. Met. Hard Mat., 19 (2001) 325-328.
[8] S. Zhang, Titanium carbonitride-based cermets: processes and properties, Materials Science and Engineering A, 163 (1993) 141-148.

[9] P. Ettmayer, H. Kolaska, W. Lengauer, K. Dreyer, Ti(C,N) Cermets - Metallurgy and Properties, International Journal of Refractory Metals and Hard Materials, 13 (1995) 343.
[10] H. Pastor, Titanium-carbonitride-based hard alloys for cutting tools, Materials Science and Engineering, 105-106 (1988) 401-409.
[11] S. Bolognini, G. Feusier, D. Mari, T. Viatte, W. Benoit, High temperature mechanical behaviour of Ti(C,N)-Mo-Co cermets, International Journal of Refractory Metals & Hard Materials, 16 (1998) 257-268.
[12] C. Mroz, Titanium diboride, American Ceramic Society Bulletin, 74 (1995) 158-159.
[13] C. Martin, B. Cales, P. Vivier, P. Mathieu, Electrical-discharge machinable ceramic composites, Materials Science and Engineering a-Structural Materials Properties Microstructure and Processing, 109 (1989) 351-356.
[14] V.J. Tennery, C.B. Finch, C.S. Yust, G.W. Clark, Science of Hard Materials, Plenum, New York, 1983.
[15] R.A. Alliegro, Encyclopedia of electrochemistry, Reinhold, New York, 1964.
[16] B.V.M. Kumar, J.R. Kumar, B. Basu, Crater wear mechanisms of TiCN-Ni-WC cermets during dry machining, International Journal of Refractory Metals & Hard Materials, 25 (2007) 392-399.
[17] E. Chicardi, F.J. Gotor, J.M. Cordoba, Enhanced oxidation resistance of Ti(C,N)-based cermets containing Ta, Corrosion Science, 84 (2014) 11-20.
[18] N.A. Abukhshim, P.T. Mativenga, M.A. Sheikh, Heat generation and temperature prediction in metal cutting: A review and implications for high speed machining, International Journal of Machine Tools and Manufacture, 46 (2006) 782-800.
[19] E. Chicardi, Y. Torres, J.M. Cordoba, P. Hvizdos, F.J. Gotor, Effect of tantalum content on the microstructure and mechanical behavior of cermets based on (TixTa1-x)(C0.5N0.5) solid solutions, Materials & Design, 53 (2014) 435-444.
[20] L. Klein, A. Bauer, S. Neumeier, M. Goeken, S. Virtanen, High temperature oxidation of gamma/gamma '-strengthened Co-base superalloys, Corrosion Science, 53 (2011) 2027-2034.
[21] Y. Niu, F. Gesmundo, F. Viani, F. Rizzo, M.J. Monteiro, The corrosion of two Co-Nb alloys under 1 ATM O-2 at 600-800 degrees C, Corrosion Science, 38 (1996) 193-211.
[22] K.T. Jacob, G. Rajitha, Role of entropy in the stability of cobalt titanates, Journal of Chemical Thermodynamics, 42 (2010) 879-885.
[23] A. Przepiera, J. Plaska, K. Przepiera, M. Jablonski, A. Konratowska, Preparation of cobalt titanates via co-precipitation while using industrial intermediates as titanium precursors, Polish Journal of Chemical Technology, 11 (2009) 51-54.
[24] T. Yamamoto, T. Ohno, Screened hybrid density functional study on Nb- and Ta-doped TiO2, Physical Review B, 85 (2012).
[25] V. Guidi, M.C. Carotta, M. Ferroni, G. Martinelli, M. Sacerdoti, Effect of dopants on grain coalescence and oxygen mobility in nanostructured titania anatase and rutile, Journal of Physical Chemistry B, 107 (2003) 120-124.
[26] M. Pfeiler, C. Scheu, H. Hutter, J. Schnoeller, C. Michotte, C. Mitterer, M. Kathrein, On the effect of Ta on improved oxidation resistance of Ti-Al-Ta-N coatings, Journal of Vacuum Science & Technology A, 27 (2009) 554-560.

FIGURE CAPTIONS.

Figure 1. Weight gain per unit area after 48 h of oxidation for all of the cermets and oxidation temperatures.

Figure 2. XRD patterns of oxidized cermets reduced to powder after the 48 h oxidation tests. (a) 800 ºC; (b) 900 ºC; (c) 1000 ºC; (d) 1100 ºC. Phases: (●) Unoxidized ceramic phase: $Ti_xTa_{1-x}C_{0.5}N_{0.5}$; (♦) Unoxidized binder phase: $Ti_xTa_{1-x}Co$; (▼) Unoxidized binder phase: $Ti_xTa_{1-x}Co_2$; (■) $Ti_xTa_{1-x}O_2$ with rutile structure; (∗) $CoTiO_3$; (♥) α-Co.

Figure 3. XRD patterns of oxidized cermets reduced to powder after the 48 h oxidation tests at 1100 ºC over the range of (110) and (211) reflections for TiO_2 and TaO_2 with the rutile structure. a) **Ti100**; b) **Ti99Ta1**; c) **Ti95Ta5**; d) **Ti90Ta10**; and e) **Ti80Ta20**.

Figure 4. XRD patterns of the surface of the oxidized cermets after the 48 h oxidation tests. (a) 800 ºC; (b) 900 ºC; (c) 1000 ºC; (d) 1100 ºC. Phases: (●) Unoxidized ceramic phase $Ti_xTa_{1-x}C_{0.5}N_{0.5}$; (o) Co_3O_4; (Δ) CoO; (■) $Ti_xTa_{1-x}O_2$ with rutile structure; (∗) $CoTiO_3$; (+) Co_2TiO_4; (♣) $CoTi_2O_5$.

Figure 5. Cross-sectional SEM images of the different cermets oxidized at 800 ºC, showing the approximate measurements of the oxidation penetration depth. The dotted lines separate the completed oxidation zones, the internal degradation zones and the unoxidized cermet areas.

Figure 6. Cross-sectional SEM images of the cermet **Ti95Ta5** oxidized at 800 ºC, 900 ºC, 1000 ºC and 1100 ºC, showing the approximate measurements of the oxidation penetration depth. The dotted lines separate the completed oxidation zones, the internal degradation zones and the unoxidized cermet areas.

Figure 7. A characteristic XEDS-SEM mapping of **Ti100** cermet oxidized at 800ºC, corroborating the clear differentiation between the oxidized / unoxidized phases and used to measure the oxidation penetration depth showed in figures 5 and 6.

Figure 8. Representative cross-sectional SEM images of cermets **Ti100** and **Ti99Ta1** showing the oxidized phases in the completed oxidation zone as determined by XEDS-SEM. a) **Ti100** at 800 ºC; b) **Ti100** at 1000 ºC; c) **Ti99Ta1** at 800 ºC; d) **Ti99Ta1** at

1000 ºC; e) **Ti99Ta1** at 1100 ºC. (1) CoO; (2) Co_3O_4; (3) TiO_2; (4) $CoTiO_3$; (5) Co_2TiO_4; (6) $CoTi_2O_5$.

Figure 9. Representative cross-sectional SEM images of cermets **Ti95Ta5**, **Ti90Ta10** and **Ti80Ta20** showing the phases in the completed oxidation zone as determined by XEDS-SEM. a) **Ti95Ta5** at 900 ºC; b) **Ti99Ta5** at 1100 ºC; c) **Ti90Ta10** at 800 ºC; d) **Ti80Ta20** at 1000 ºC; e) **Ti90Ta10** at 1000 ºC. (1) CoO; (3a), (3b) and (3c) $Ti_xTa_{1-x}O_2$; (4) $CoTiO_3$; (5) Co_2TiO_4.

Figure10. Representative cross-sectional SEM images of the internal degradation zone [a) **Ti100** at 1000 ºC; b) **Ti99Ta1** at 1000 ºC; c) **Ti95Ta5** at 1100 ºC] and the oxidation front [d) **Ti100** at 900 ºC; e) **Ti80Ta20** at 1100 ºC] for the different oxidized cermets, showing the phases in these regions as determined by XEDS-SEM. (3) $Ti_xTa_{1-x}O_2$ (7) α-Co.

Figure 11. Representative semi-quantitative XEDS-SEM spectra of oxidized phases found in the different areas analyzed and previously detected by XRD.

TABLES.

Table 1. Percentage reduction of the weight gain per unit area for each cermet at each oxidation temperature compared to the weight gain per unit area of the **Ti100** cermet (reference material) after the 48h oxidation tests.

Cermet	800ºC	900ºC	1000ºC	1100ºC
Ti100	-	-	-	-
Ti99Ta1	67.2	67.2	48.0	46.3
Ti95Ta5	89.2	90.7	84.9	72.8
Ti90Ta10	94.1	94.2	89.3	85.6
Ti80Ta20	95.6	96.3	94.0	92.8

Table 2. Lattice parameters for the $Ti_xTa_{1-x}O_2$ solid solution with rutile-type structure determined from the X-ray diffractograms of cermets oxidized at 1100ºC.

Cermet	a=b (Å)	c (Å)
Ti100	4.5933	2.9592
Ti99Ta1	4.5935	2.9608
Ti95Ta5	4.6025	2.9666
Ti90Ta10	4.6139	2.9761
Ti80Ta20	4.6314	2.9823

Table 3. Punctual semi-quantitave compositions calculated from XEDS-SEM spectra performed in different zones of the oxide scale and internal oxidation region of the oxidized cermets. The numbers in figures 8-10 mark the analyzed zones. The nature of phases that best suits the results of the analyses is also shown.

Zone	Ti (at%)	Ta (at%)	Co (at%)	O (at%)	Approximate phase stoichiometry
1	-	-	50.4	49.6	CoO
2	-	-	58.4	41.6	Co_3O_4
3	34.3	-	-	65.7	TiO_2
3a	28.1	1.7	-	70.2	$Ti_xTa_{1-x}O_2$
3b	25.5	4.8	-	69.7	
3c	20.8	8.8	-	70.4	
4	24.7	-	22.7	52.6	$CoTiO_3$
5	15.8	-	29.6	54.6	Co_2TiO_4
6	25.4	-	13.1	61.5	$CoTi_2O_5$
7	3.9	1.3	94.8	-	α-Co

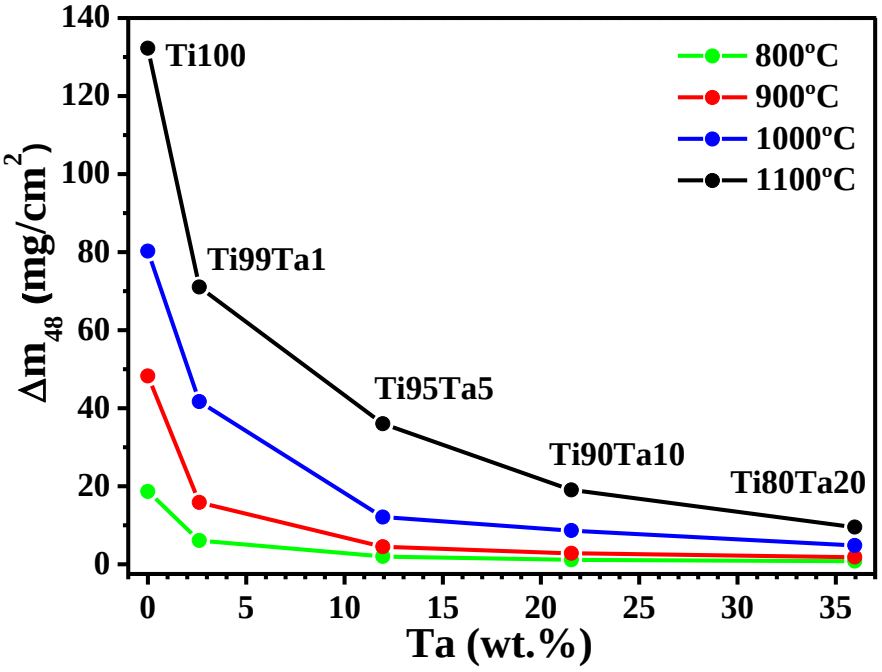
140
120
100
80
60
40
20
0
0
5
10
15
20
25
30
35
Ta (wt.%)
Δm48 (mg/cm2)
Ti100
Ti99Ta1
Ti95Ta5
Ti90Ta10
Ti80Ta20
800°C
900°C
1000°C
1100°C

Figure 1

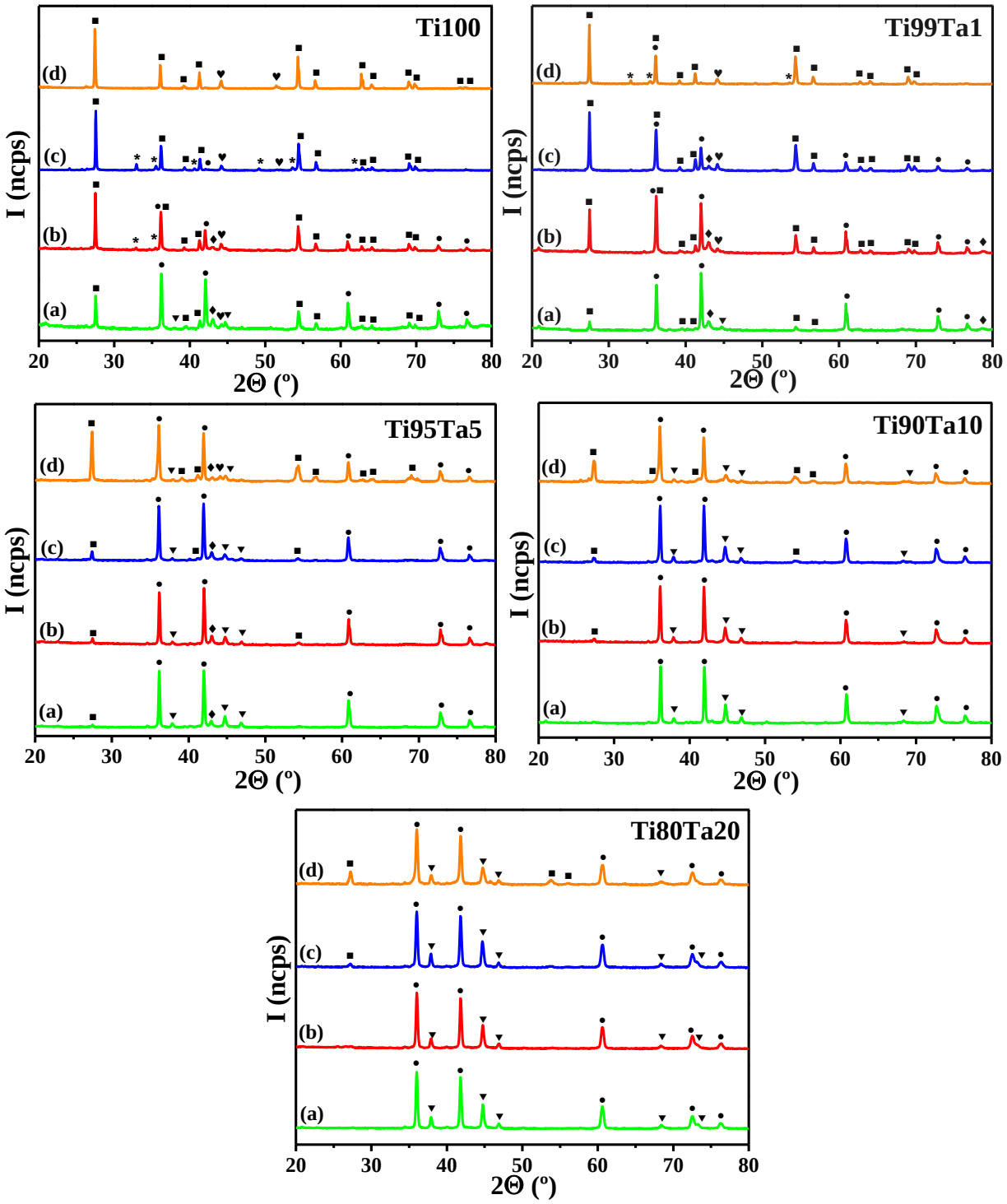
Ti100
Ti99Ta1
Ti95Ta5
Ti90Ta10
Ti80Ta20
(a)
(b)
(c)
(d)
I (ncps)
2Θ (º)
20
30
40
50
60
70
80

Figure 2

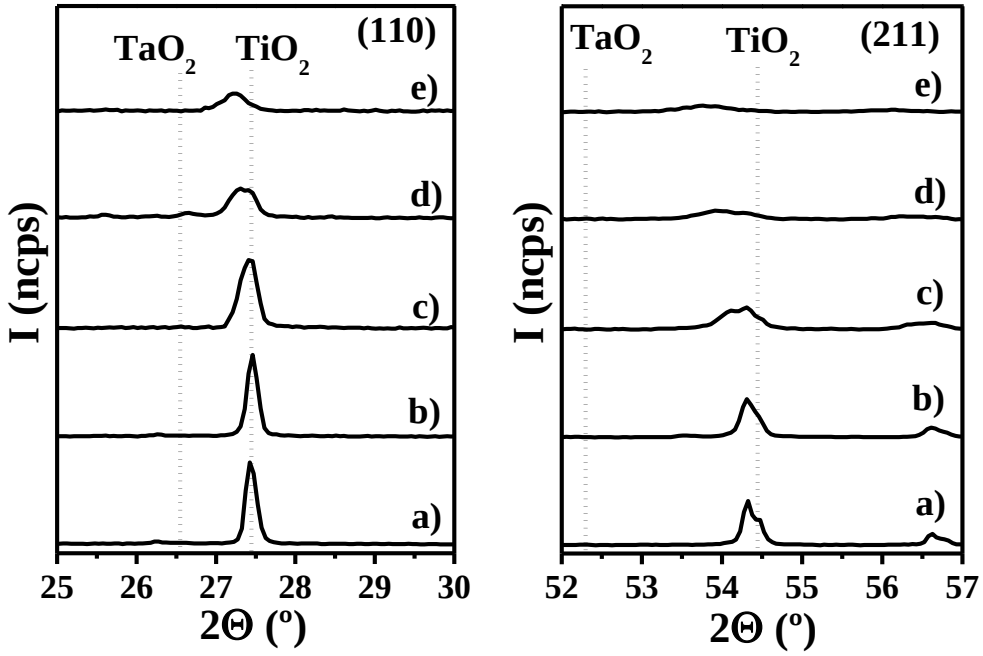
TaO2
TiO2
(110)
e)
d)
c)
b)
a)
I (ncps)
25
26
27
28
29
30
2Θ (º)
TaO2
TiO2
(211)
e)
d)
c)
b)
a)
I (ncps)
52
53
54
55
56
57
2Θ (º)

Figure 3

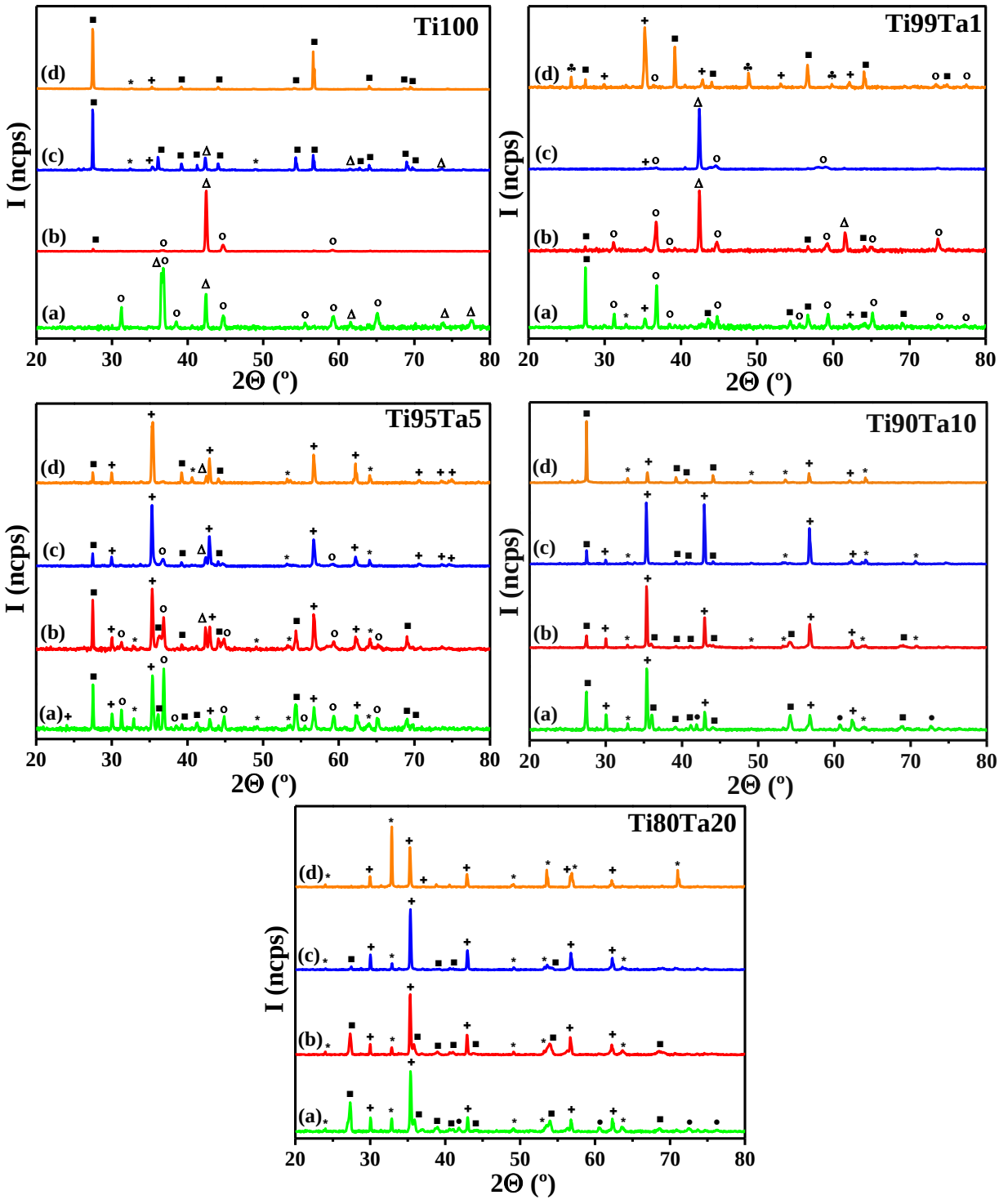
Ti100
Ti99Ta1
Ti95Ta5
Ti90Ta10
Ti80Ta20
(a)
(b)
(c)
(d)
I (ncps)
2Θ (º)
20
30
40
50
60
70
80

Figure 4

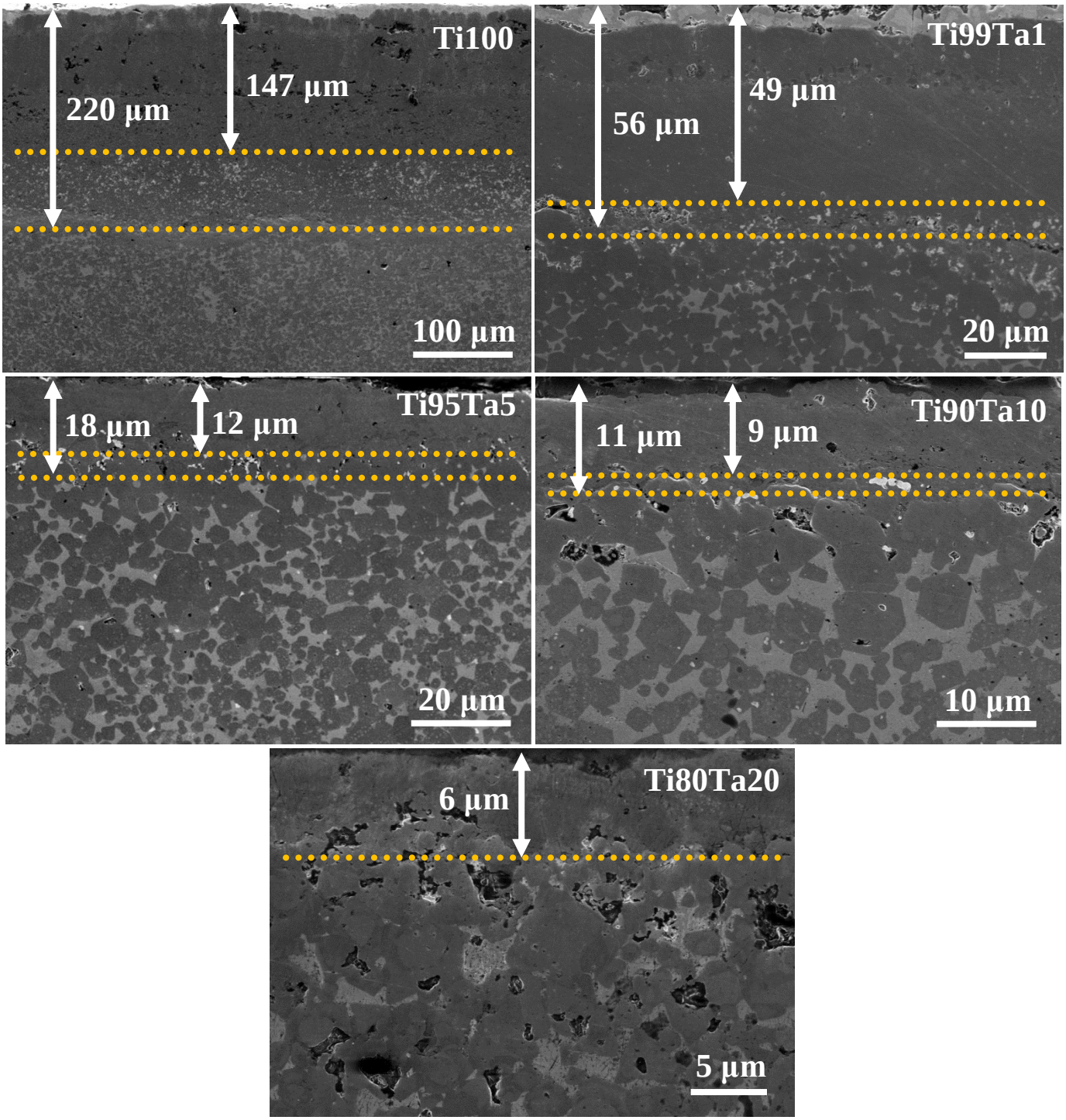
Ti100
220 µm
147 µm
100 µm
Ti99Ta1
56 µm
49 µm
20 µm
Ti95Ta5
18 µm
12 µm
20 µm
Ti90Ta10
11 µm
9 µm
10 µm
Ti80Ta20
6 µm
5 µm

Figure 5

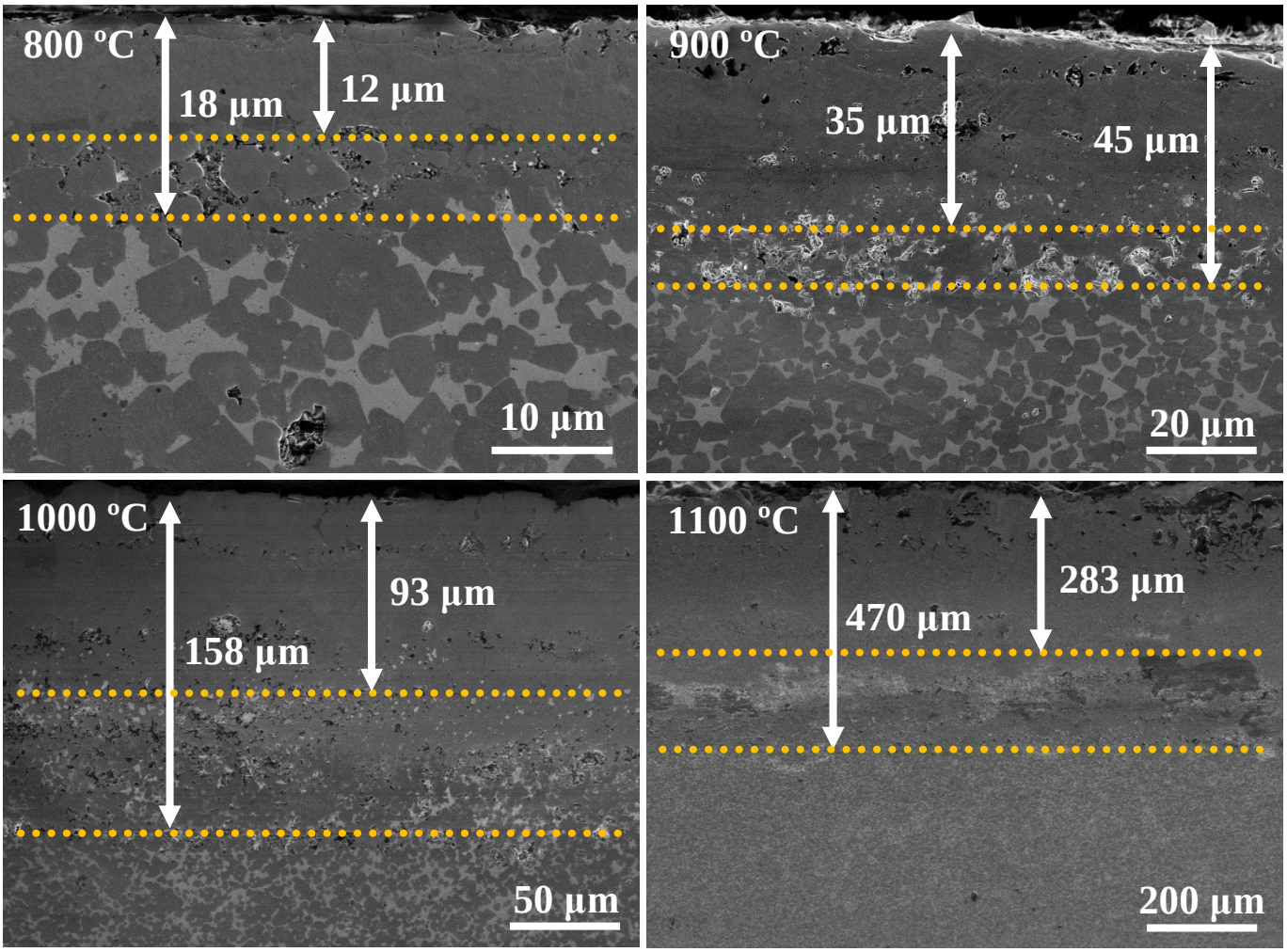
800 °C
18 µm
12 µm
10 µm
900 °C
35 µm
45 µm
20 µm
1000 °C
158 µm
93 µm
50 µm
1100 °C
470 µm
283 µm
200 µm

Figure 6

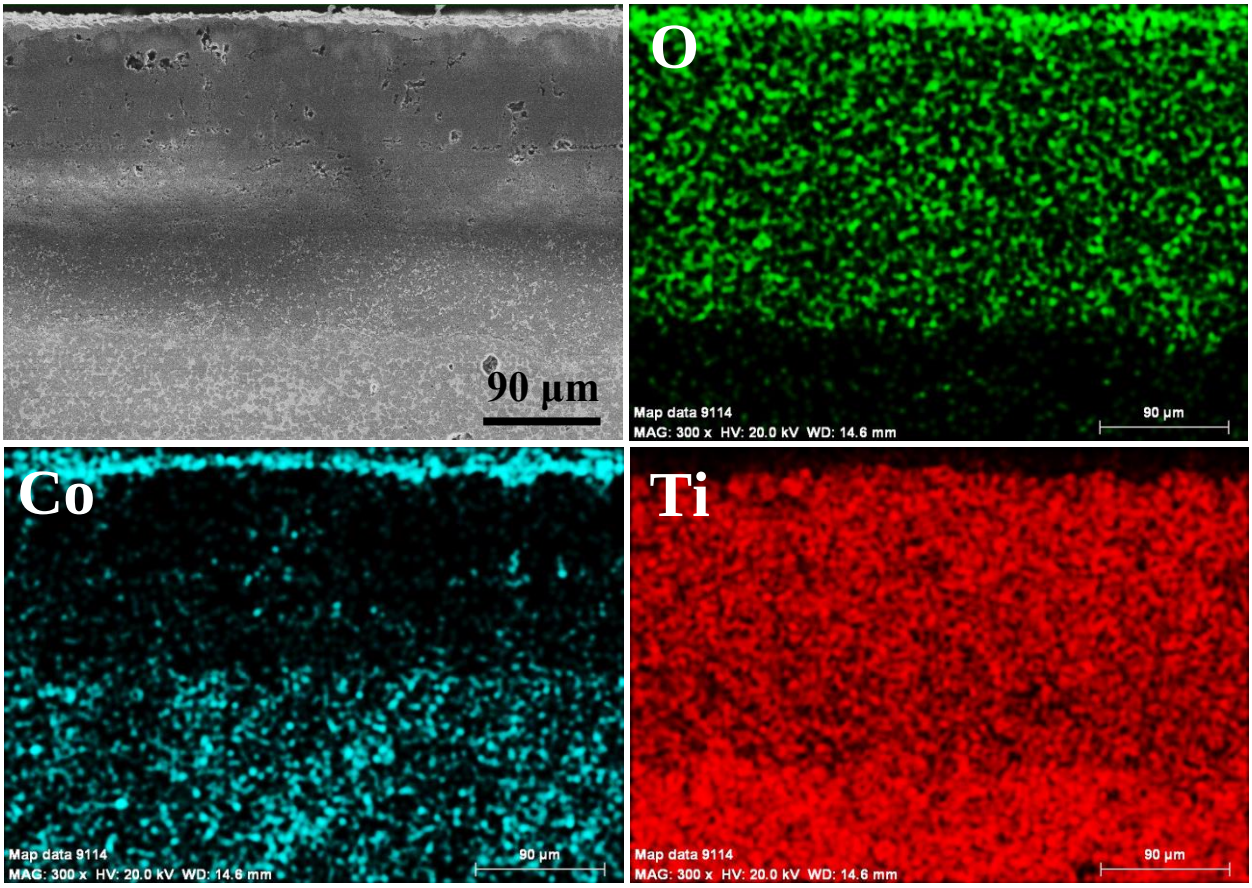
90 µm
O
Map data 9114
MAG: 300 x HV: 20.0 kV WD: 14.6 mm
90 µm
Co
Map data 9114
MAG: 300 x HV: 20.0 kV WD: 14.6 mm
90 µm
Ti
Map data 9114
MAG: 300 x HV: 20.0 kV WD: 14.6 mm
90 µm

Figure 7

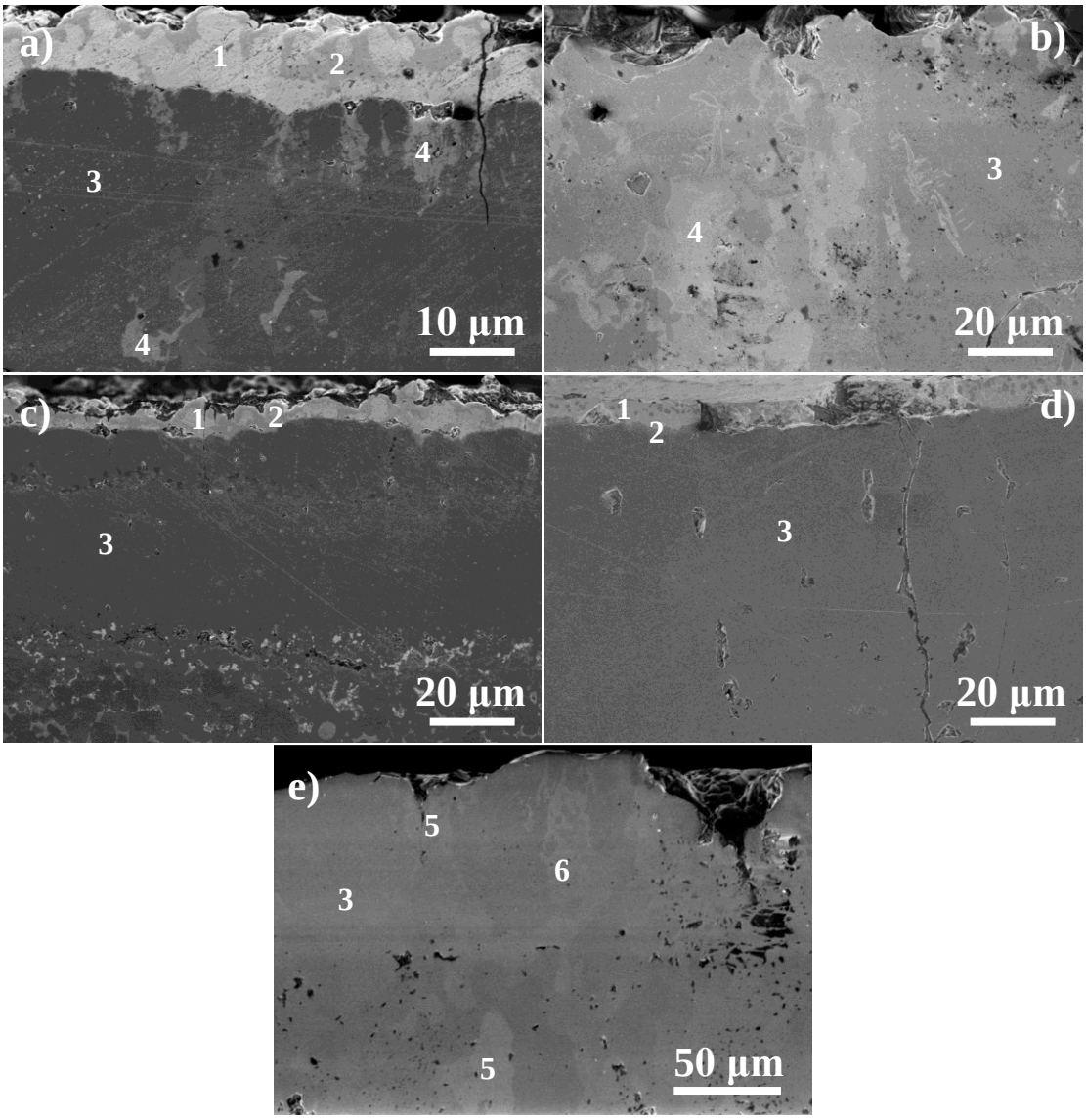

Figure 8

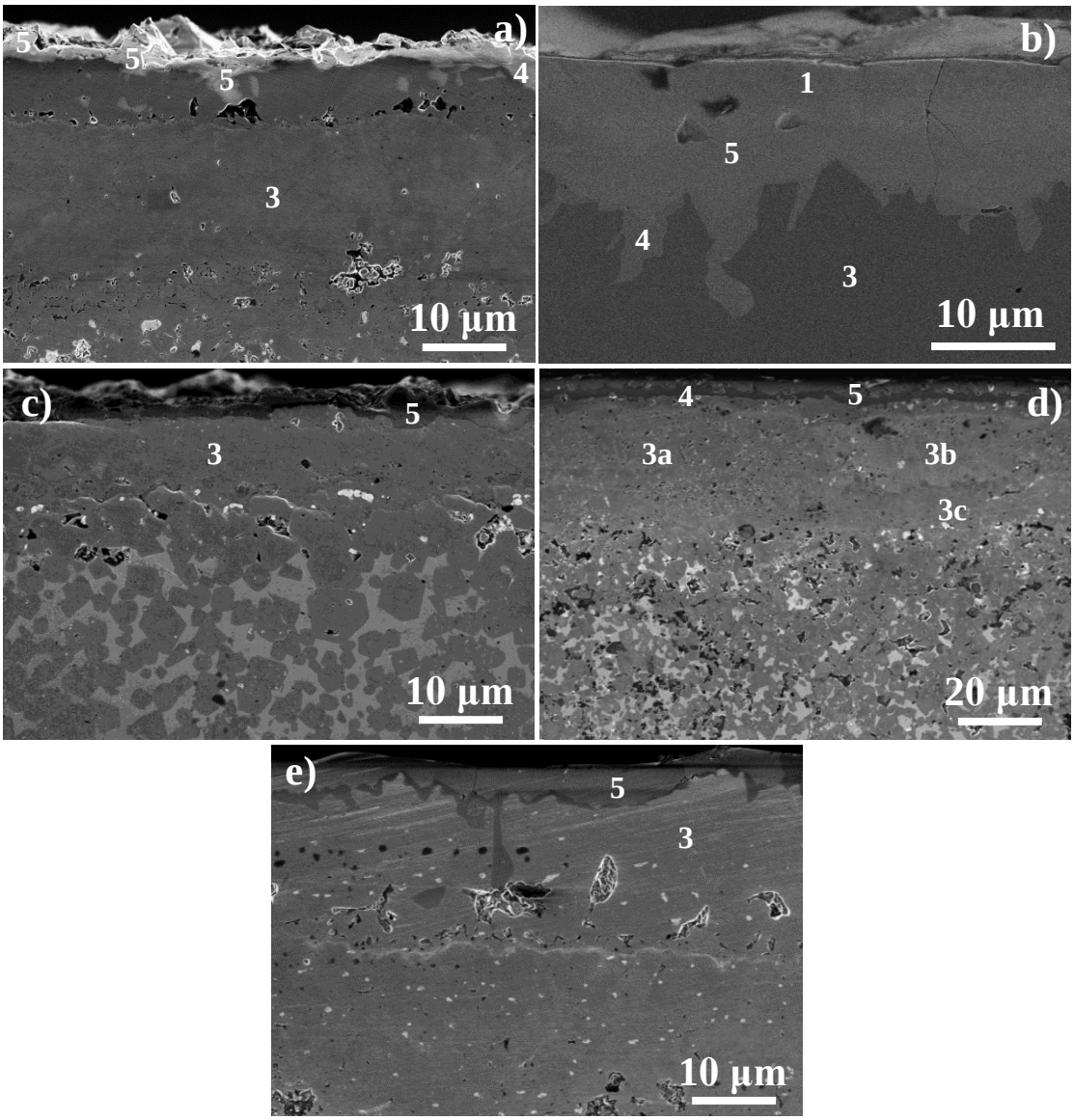

Figure 9

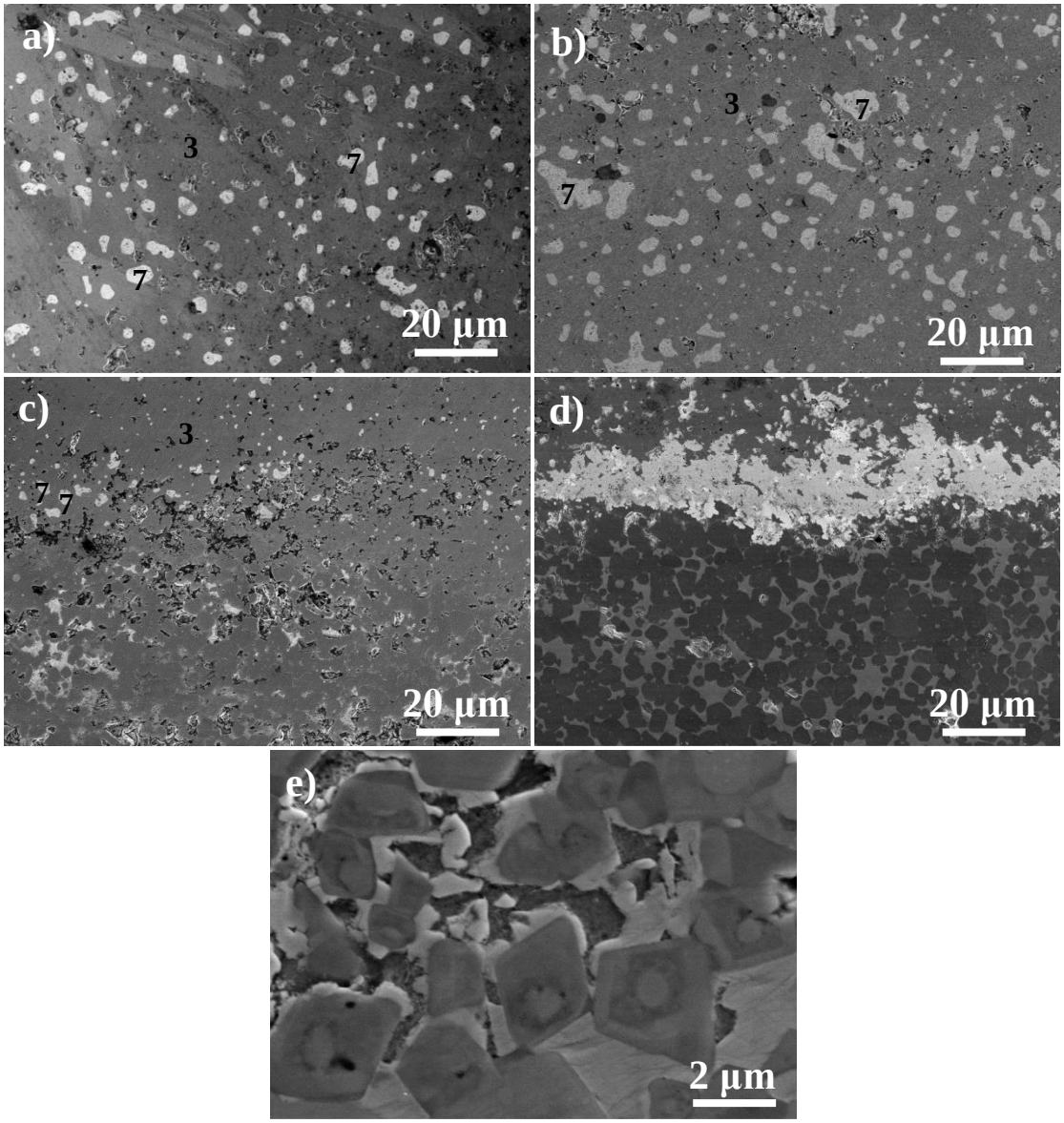

Figure 10

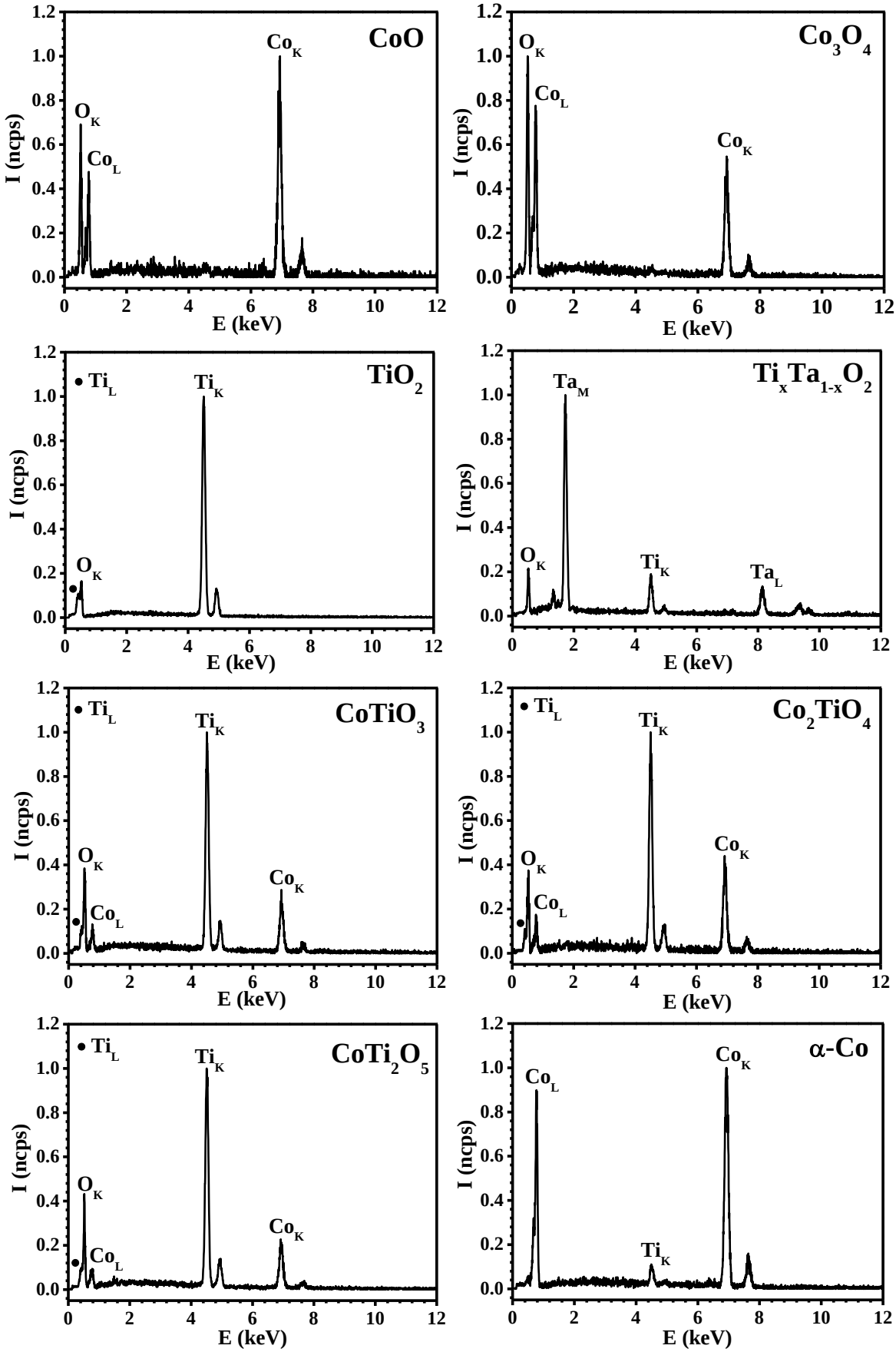
CoO
Co_K
O_K
Co_L
Co_3O_4
O_K
Co_L
Co_K
TiO_2
Ti_L
Ti_K
O_K
Ti_xTa_1-xO_2
Ta_M
O_K
Ti_K
Ta_L
CoTiO_3
Ti_L
Ti_K
O_K
Co_K
Co_L
Co_2TiO_4
Ti_L
Ti_K
Co_K
O_K
Co_L
CoTi_2O_5
Ti_L
Ti_K
O_K
Co_K
Co_L
α-Co
Co_L
Co_K
Ti_K
I (ncps)
E (keV)

Figure 11